The 9th European Congress on Computational Methods in Applied Sciences and Engineering
ECCOMAS Congress 2024
3 – 7 June 2024, Lisboa, Portugal

OPTIMAL MATERIAL SELECTION APPLIED TO FUNCTIONALLY GRADED BEAMS FOR STRESS MINIMIZATION

RUI F. SILVA[1], PEDRO G. COELHO[1,2,3], FÁBIO M. CONDE[1,3], CLÁUDIA J. ALMEIDA[1] AND CAROLINA V. GUSTAVO[1]

[1] UNIDEMI, Department of Mechanical and Industrial Engineering, NOVA School of Science and Technology, Universidade NOVA de Lisboa, 2829-516 Caparica, Portugal

[2] IDMEC, Instituto Superior Técnico, Universidade de Lisboa, Av. Rovisco Pais 1, Lisbon 1049-001, Portugal

[3] LASI, Intelligent Systems Associate Laboratory, 4800-058 Guimarães, Portugal

e-mails: rmfd.silva@campus.fct.unl.pt; pgc@fct.unl.pt; f.conde@fct.unl.pt; csj.almeida@campus.fct.unl.pt; c.gustavo@campus.fct.unl.pt.

Key words: Beam, Composites, Functionally Graded Material, Stress, Topology Optimization

Summary. The multi-material design setting offers additional design freedom, which can lead to structures with lower stress levels compared to the single-material case. The present work is focused on multi-material stress-based topology optimization. Specifically, the maximum von Mises stress is minimized inside a design domain through material selection. Two solid materials are mixed to generate an advanced composite, i.e., a Functionally Graded Material (FGM). The FGM's mechanical properties are here provided by the well-known RAMP interpolation scheme, which falls within the Hashin-Shtrikman bounds for the elastic moduli of isotropic composite materials. The proposed stress-based formulation is applied to a beam under pure bending. From a manufacturing standpoint, this example is possibly the easiest one to fabricate, since the FGM solution corresponds to a layer-by-layer gradation of properties (concept of layer-wise FGM). The change (or gradient) in the material property is unidirectional along the vertical direction of the beam only. The obtained FGM beam leads to evenly distributed stresses of lower magnitude, apart from the neutral surface zone, when compared to the classical linear stress distribution of the homogeneous beam. The FGM beam deformed shape is also presented and compared to the homogeneous case.

1 INTRODUCTION

Due to the advent of new manufacturing techniques, materials science has foreseen a transition from conventional metals to advanced composites and smart materials. In this context, a new class of composite materials, known as Functionally Graded Materials (FGMs), has received significant attention from the scientific community due to the FGM's intrinsic mechanical performance. The concept of FGMs was first introduced in Japan in 1984 by a group of researchers for the development and application of thermal barrier materials [1].

Basically, FGMs are advanced engineering materials designed for a specific performance or function in which a spatial gradation in structure and/or composition lend itself to tailored properties. Over traditional composites, FGMs improve structural strength by replacing sharp interfaces with gradually changing interfaces, producing then a smooth transition between two distinct materials. Additionally, FGMs can achieve tailored structural properties in specific directions. These advantages have driven the research and development of FGMs for various high-tech applications, including aerospace, bioengineering, and the nuclear industry.

In recent years, there has been a growing trend of designing FGMs through Topology Optimization (TO). TO aims to find the optimal material layout within a given design space for a given set of loads, boundary conditions, and constraints, with the goal of maximizing performance or minimizing material usage. By iteratively adjusting the distribution of material, TO can create highly efficient structures that often feature complex and organic shapes, which makes it a powerful tool in engineering and architectural applications for developing innovative and lightweight designs. Although TO may render very efficient design solutions, they often present geometrical complexity which challenges their manufacture. In fact, the current state-of-the-art on available manufacturing technologies may prevent attaining the extreme (optimal) predicted performance levels obtained by TO [2].

Beams are one of the main structures in mechanical engineering designed primarily to resist loads applied perpendicular to their longitudinal axis. Many studies on FGM beams use power-laws to impose the material gradient along one direction, e.g., the transverse (thickness) direction or axial (length) direction, so-called Uni-directional (UD) FGM beams [3-4]. Due to the limited precision of the manufacturing equipment, these layer-wise FGMs emerge as ideal candidates for manufacturing and thus warrant particular focus. The first attempt on an elasticity solution of FGM beams subjected to static transverse loads was proposed by Sankar [5] assuming the beam properties to vary through thickness following an exponential-law. Many works have since followed this thematic [6-9]. These previous references primarily focus on the modelling and analysis of FGM beams, yet optimization remains a significant and relevant issue. Many researchers have applied optimization to FGM beams for different objectives. For instance, Noh et al. [10] employed the Reliability Based Design Optimization (RBDO) method to minimize thermal stresses in FGM beams under thermal loads. Meanwhile, Taheri and Hassani [11] focused on minimizing the mass of a clamped-clamped FGM beam with an eigen-frequency constraint. In the field of TO, Xia and Wang [12] developed a level set based optimization approach with the aim of minimizing the compliance of FGM beams. Maleki Jebeli and Shariat Panahi [13] integrated their Bi-directional Evolutionary Structural Optimization (BESO) method with GA to prove the outperformance of their methodology over that of Xia and Wang [12]. Later, Almeida et al. [14] implemented the Continuous Approximation of Material Distribution (CAMD) method for TO of FGM beams subjected to thermal and mechanical loads. Their aim was to find the best material distribution for such materials, which resulted in the minimum compliance of the beams taking into consideration symmetry and pattern repetition constraints. More recently, Cheng et al. [15] proposed an efficient Collaborative Robust Topology Optimization (CRTO) method considering hybrid bounded uncertainties applied to several numerical examples, including the MBB beam. Both the relative density of every finite element and the volume fraction of reinforcement in each layer are regarded as design variables in the SIMP-based CRTO process of FGMs. In addition, Silva et al. [16] solved the maximum von Mises stress minimization problem for a beam under

pure bending using an FGM material model, which led to a layer-wise FGM beam solution with a lower peak stress compared to the homogenous beam counterpart.

The present work applies TO techniques to determine the optimal pointwise material distribution of a beam subject to pure bending in order to minimize the maximum von Mises stress. The optimal solution of this optimization problem is a layer-wise FGM (easy-to-manufacture design), as all stresses are unidirectional (normal to the cross-section of the beam). Conceptually, material gradation along the beam's height redistributes stresses, reducing them as shown in this work. Afterwards, the stress distribution and deformed shape of the obtained FGM beam are shown and further discussed.

The remainder of the paper is organized as follows. Section 2 presents the material model within the framework of material selection optimization. The problem statement is presented in Section 3. The sensitivity analysis of stress w.r.t. density is in Section 4. Section 5 shows the numerical results, including an FGM beam design (layer-wise FGM) and the corresponding property post-processing, as well as the stress and displacement analyses of such FGM design. Finally, Section 6 points out conclusions.

2 MATERIAL MODEL

Consider the in-plane arbitrary shape of an elastic body in Figure 1, under an applied external traction load $\mathbf{t}$ on the boundary segment $\Gamma_t \subset \partial\Omega$ of the reference domain Ω, with fixed displacement boundary conditions on segment Γ_u. Within Ω, two subregions can be distinguished: (1) a non-design region, Ω^{nd}, which can be solid (black) or void (white); and (2) a design region (gray), Ω^{d}, wherein optimal material selection takes place in order to find the FGM that minimizes the peak stress in the structure.

As sketched in Figure 1, the reference domain Ω is discretized by a Finite Element (FE) mesh. Each design element of Ω^{d} is associated with a density design variable, which is assumed constant within that element. There are as many design variables as the number of elements discretizing Ω^{d}. This design variable sets the volume fraction (between 0 and 1) of one of the two materials mixed together to form an FGM. In this case, one assumes that such volume fraction (e.g., 0.3) corresponds to the stiffest material volume fraction, i.e., Mat 1. The respective complement (e.g., 0.7) is the Mat 2 volume fraction. This way, the optimization problem based on such density variables is, in fact, a material selection problem of pointwise choice of compositional grading across the structure's design domain Ω^{d}, so-called FGMO problem in Section 3. The type of FGM generated in this problem features a gradient in material composition, in contrast to other types of FGM that might alternatively involve gradients in porosity or microstructure. The variation of the material property (Young's Modulus in this case) within the interval of the material volume fraction is thus an important data that should be available in practice to serve as an input for the FGM computational design. Typically, this is an experimental type of data, obtained from mechanical testing of samples. Each sample corresponds to the deposition of a specific composition (e.g., 0% Mat 1 with 100% Mat 2, 10% Mat 1 with 90% Mat 2, and so forth, till 100% Mat 1 and 0% Mat 2) in a layer-wise fashion resorting to additive manufacturing.

In this work, it is assumed that the mixture of two solid materials is possible for the entire volume fraction range (or composition percentages). The success of mixing dissimilar materials is out of the scope of this work. In fact, it raises important metallurgy issues that warrant in-

depth research work, particularly in the field of materials science. For now, a preliminary approach based entirely on computational design under a few hypotheses is presented. Such approach can be applied either to metals or polymers and considering different Young's Modulus ratios. In the absence of experimental data, which is the case in the present framework, the properties of solid mixtures can be predicted by the Hashin-Shtrikman (HS) bounds [17] for the elastic moduli of isotropic composite materials. These theoretical bounds depend on the volume fractions of each constituent materials, while assuming they are mixed uniformly with no microstructure (homogeneous resulting solid). The average of such bounds is approximated here by the RAMP interpolation scheme [18], given by:

$$\mathbf{E} = \left[\frac{\rho}{1 + 1.0399(1-\rho)}\mathbf{E}_1 + \left(1 - \frac{\rho}{1 + 1.0399(1-\rho)}\right)\mathbf{E}_2\right] \tag{1}$$

where $\rho \in [10^{-3}, 1]$ is the density design variable for the material selection purpose, and $\mathbf{E}_1$ and $\mathbf{E}_2$ are the isotropic stiffness tensors of the stiffest (Mat 1) and weakest (Mat 2) solid phases, respectively.

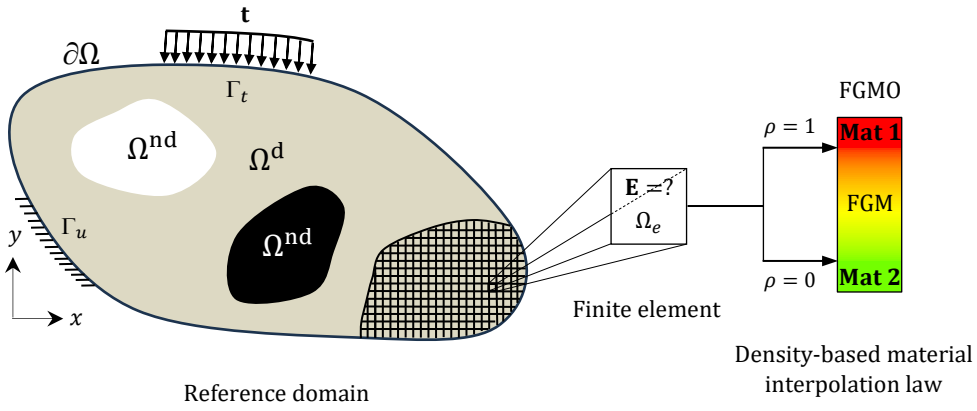

Figure 1 Arbitrary domain, presenting design and non-design subregions, with a FE mesh, where a density-based variable, per element, measures the volume fraction of one of the two constituents mixed to render a compositional grading across Ω.

3 OPTIMIZATION PROBLEM

In the present framework, the minimization of the maximum von Mises stress, σ_e^{VM}, in the structure's domain is sought [16,19-20]. However, a min–max problem raises non-differentiability issues. To tackle this, the so-called bound formulation, as suggested by Taylor and Bendsøe [21], is adopted here. This means replacing the objective function $\max(\sigma^{\mathrm{VM}})$ by the function z to be minimized on the design variables, i.e., the original ones, plus another one that is the z itself, with $z \in]0, +\infty[$. The search is carried out within an enlarged constraint set to include $\sigma^{\mathrm{VM}} < z$, where z here means the stress limit. The original points of non-differentiability correspond now to corners in the constraint set of the enlarged space and arise from intersections of differentiable constraints. Many constraints thus appear now in the

problem statement, but that also means stresses are treated as they are, i.e., local, which allows skipping here any aggregation method that could otherwise compromise pointwise control of stresses.

The stress-based problem formulation in this work comprises the material selection density variables, $\boldsymbol{\rho}$, and the artificial design variable, z. The problem at hand is thus a material optimization problem, denoted here as Functionally Graded Material Optimization (FGMO). Basically, this means that each point of the structure's design domain is a material point (no void), and thus the problem only involves the pointwise selection of material. The topology of the structure is fixed. This optimization problem is formulated as follows:

$$\min_{\boldsymbol{\rho},z} z \tag{2a}$$

$$\text{s.t.}$$

$$\frac{\sigma_e^{\mathrm{VM}}(\mathbf{u}(\boldsymbol{\rho}),\boldsymbol{\rho})}{z} \leq 1, \quad e = 1,\dots,N^{\mathrm{d}} \tag{2b}$$

where $\mathbf{u}$ is the displacement field obtained by solving the equilibrium equation $\mathbf{K}\mathbf{u} = \mathbf{f}$ and N^{d} is the number of design elements present in the FE mesh. The stress constraints (2b) are written according to the input format of constraints as adopted by MMA (Fortran version) [22], i.e., $\mathrm{g} \leq 1$.

4 STRESS SENSITIVY ANALYSIS

This work uses the Method of Moving Asymptotes (MMA, [22]), as the optimizer, to solve the proposed stress-based problem (2). Since this is a gradient-based optimizer, one needs to perform sensitivity analysis.

In the equations below, indexes $i, e \in \{1,\dots,N^{\mathrm{d}}\}$ correspond to the design FE index, and indexes $z, j, k, l \in \{1,2\}$ are related to the coordinate system directions considering 2D problems. Regarding the calculation of the von Mises stress sensitivity with respect to (w.r.t.) the design variables ρ_i, the adjoint method [23] is applied. As for the stress derivatives w.r.t. the design variable z, they are trivial and thus skipped here.

Assuming a FE discretization of the reference domain Ω, the total derivative of the von Mises stress, $\sigma_e^{\mathrm{VM}} = \sigma_e^{\mathrm{VM}}\big(\boldsymbol{\rho}, \mathbf{u}(\boldsymbol{\rho})\big)$, at element e, depends explicitly and implicitly on the design variables ρ_i, such that:

$$\frac{\mathrm{d}\sigma_e^{\mathrm{VM}}}{\mathrm{d}\rho_i} = \frac{\partial \sigma_e^{\mathrm{VM}}}{\partial \rho_i} - \boldsymbol{\lambda}^{\mathrm{T}} \frac{\partial \mathbf{K}}{\partial \rho_i} u_k \tag{3}$$

where the vector $\boldsymbol{\lambda}$ is the adjoint variable that solves the following adjoint problem:

$$\mathbf{K}\boldsymbol{\lambda} = \left(\frac{\partial \sigma_e^{\mathrm{VM}}}{\partial \mathbf{u}}\right) \tag{4}$$

In the Finite Element Method (FEM), the displacements in nodes **u** are multiplied by shape functions ϕ_α in order to estimate the displacement at any point in the domain of the considered element:

$$u_k = \bar{u}_{k\alpha}\phi_\alpha \tag{5}$$

where $\alpha \in \{1, \dots, 8\}$ is the node number of the 8-node isoparametric quadrilateral FE (Q8) used in this work. Therefore, the von Mises stress derivative w.r.t. displacements **u** in (4) is given by:

$$\frac{\partial \sigma_e^{\mathrm{VM}}}{\partial \bar{u}_{k\alpha}} = \frac{\int_{\Omega_e^{\mathrm{d}}} \frac{1}{2}\left[\left(\frac{\partial \sigma_{11}^e}{\partial \bar{u}_{k\alpha}} - \frac{\partial \sigma_{22}^e}{\partial \bar{u}_{k\alpha}}\right)(\sigma_{11}^e - \sigma_{22}^e) + \frac{\partial \sigma_{11}^e}{\partial \bar{u}_{k\alpha}}\sigma_{11}^e + \frac{\partial \sigma_{22}^e}{\partial \bar{u}_{k\alpha}}\sigma_{22}^e + 6\frac{\partial \sigma_{12}^e}{\partial \bar{u}_{k\alpha}}\sigma_{12}^e\right] \mathrm{d}\Omega_e^{\mathrm{d}}}{\left|\Omega_e^{\mathrm{d}}\right| \sqrt{\frac{1}{2}[(\sigma_{11}^e - \sigma_{22}^e)^2 + (\sigma_{11}^e)^2 + (\sigma_{22}^e)^2] + 3(\sigma_{12}^e)^2}} \tag{6}$$

In order to compute the von Mises stress derivative w.r.t. displacements (6), the Hooke's law derivative w.r.t. displacements **u** must be computed first, which gives:

$$\frac{\partial \sigma_{zj}^e}{\partial \bar{u}_{k\alpha}} = E_{zjkl}\frac{\partial \phi_\alpha}{\partial x_l} \tag{7}$$

As regards the explicit part of the total derivative of the von Mises stress w.r.t. ρ_i, one obtains:

$$\frac{\partial \sigma_e^{\mathrm{VM}}}{\partial \rho_i} = \frac{\int_{\Omega_e^{\mathrm{d}}} \frac{1}{2}\left[\left(\frac{\partial \sigma_{11}^e}{\partial \rho_i} - \frac{\partial \sigma_{22}^e}{\partial \rho_i}\right)(\sigma_{11}^e - \sigma_{22}^e) + \frac{\partial \sigma_{11}^e}{\partial \rho_i}\sigma_{11}^e + \frac{\partial \sigma_{22}^e}{\partial \rho_i}\sigma_{22}^e + 6\frac{\partial \sigma_{12}^e}{\partial \rho_i}\sigma_{12}^e\right] \mathrm{d}\Omega_e^{\mathrm{d}}}{\left|\Omega_e^{\mathrm{d}}\right| \sqrt{\frac{1}{2}[(\sigma_{11}^e - \sigma_{22}^e)^2 + (\sigma_{11}^e)^2 + (\sigma_{22}^e)^2] + 3(\sigma_{12}^e)^2}} \tag{8}$$

where the Hooke's law is here differentiated again to obtain the needed stress derivatives w.r.t. ρ_i, which gives:

$$\frac{\partial \sigma_{zj}^e}{\partial \rho_i} = \frac{\partial E_{zjkl}}{\partial \rho_i}\varepsilon_{kl}\delta_{ie} \tag{9}$$

where **δ** is the Kronecker delta. The derivative of the stiffness tensor **E** simply involves the straightforward derivative of Eq. (1), which is trivial and thus skipped here.

5 NUMERICAL RESULTS

To demonstrate the application of the proposed stress-based formulation (2), a two-dimensional beam is presented in Figure 2. All dimensions are indicated in meters. To simplify, the thickness of the beam is assumed unitary. Plane stress is assumed. To generate a torque of

$100\ \text{kN}\cdot\text{m}$, such that the beam is subject to pure bending at the mid-span, one applies two loads of magnitude $F = 142.857\ \text{kN}$. The beam is meshed with 126×30 8-node isoparametric quadrilateral FEs. Due to symmetry, only half of the beam will be modelled, which helps reducing the number of design variables and stress constraints. For the sake of generalization, normalized material properties are used as the problem input data instead of absolute values. Specifically, Mat 1 has a Young's Modulus of $E_1 = 1$ GPa, while Mat 2 has a Young's Modulus of $E_2 = 0.34$ GPa. The Poisson's ratio of both materials is assumed equal to 0.3. All stress results in this section are always to be read in MPa units.

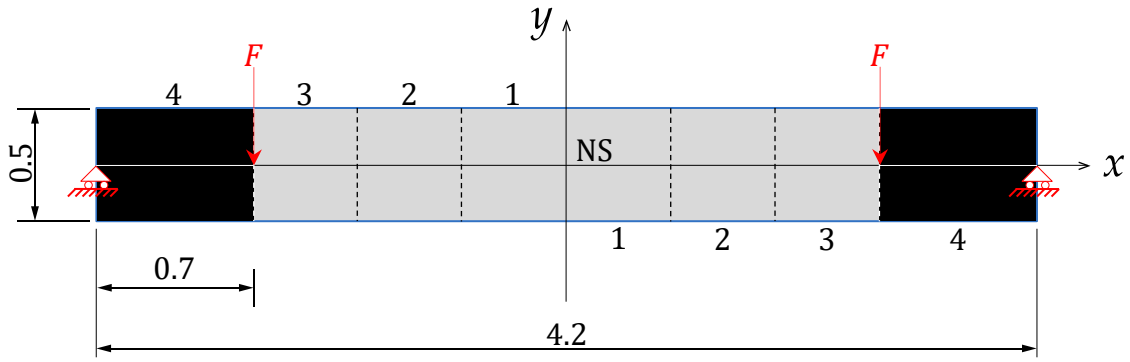

Figure 2 Two-dimensional beam subject to pure bending at the mid-span.

In the example presented in this section, the Neutral Surface (NS) coincides with the centroid of the beam's cross-section, allowing for the coupling (or grouping) of design variables in elements opposite to the NS. This further reduces the number of design variables and von Mises stress constraints, which are inputs to the optimizer. Moreover, the initial design for the optimization considers $\boldsymbol{\rho} = 0.5$, except for the extreme (top or bottom) beam layers, where $\boldsymbol{\rho} = 10^{-3}$.

5.1 OPTIMAL FGM

As depicted in Figure 2, each side of the beam w.r.t. the symmetry line is divided into four regions as follows. Region 4 is a homogeneous non-design solid region, composed of the stiffest base material (fixed $\rho = 1$), and it represents 1/3 of half of the beam's length, i.e., 0.7 m. Regions 1-3 (in gray) identify the design domain and their combined length is 2/3 of half of the beam's length, i.e., 1.4 m . In turn, each one of these 1-3 regions has a length of $2/9$ of half of the beam's length, i.e., 0.46667 m .

The interface between the design and non-design regions (transition zone between regions 3-4) generates a non-smooth variation (or perturbation) of the stress field. Therefore, the related stress peaks therein could easily unduly occupy the optimizer in region 3 to render the FGM that best mitigates such stress concentrations. That is not the purpose of this example. Instead, the goal is to modify the purely linear stress distribution associated with pure bending on account of an FGM and see strength improvements compared to the original homogenous beam case. For that purpose, and bearing in mind the Saint-Venant's principle, one simply minimizes the maximum von Mises stress only inside regions 1 and 2 (far away enough from

the transition zone between regions 3-4). This way, one avoids the algorithm being trapped in reducing stresses of the unwanted transition zone 3. Hence, the free design allowed in zone 3 is only expected to promote stress uniformity in regions 1-2. Importantly, one realizes that stress sensitivities w.r.t. densities consider that the design variables embrace not only regions 1 and 2, but also region 3. To sum up, the FGM regions of interest are regions 1 and 2 only.

From a manufacturing standpoint, this example is possibly the easiest one to fabricate since the FGM solution here corresponds to a layer-by-layer gradation of properties (concept of layer-wise FGM), where material uniformity along the horizontal direction exists and property changes (or gradient) are only obtained along the beam's vertical direction. Fairly enough, by observing the optimization result in Figure 3, the material gradation in region 2 may still appear perturbed, as region 3 may not fully absorb the cross-section discontinuity effects. Therefore, the desired FGM solution of interest (layer-wise) is purely obtained in region 1. The results for the full-length of the beam are simply provided here for the sake of transparency. In between regions 1 and 4, perturbations are expected, but not relevant to comprehend the benefits of the intended layer-wise FGM here. Finally, one can see that a beam under pure bending is a very interesting example here, as it renders a unidirectional property gradient (layer-wise) as the simplest proof-of-concept on FGMs mitigating stresses.

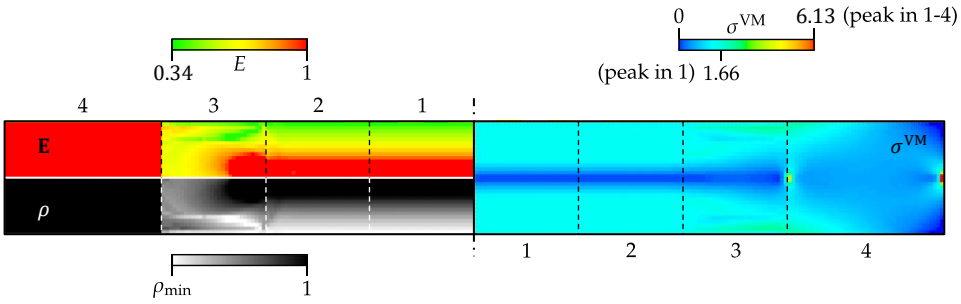

Figure 3 Stress-based FGMO result for the beam sketched in Figure 2. Young's Modulus, density and stress maps. The peak stresses obtained among all regions, as well as in region 1 only, are highlighted at the stress color scale.

From a stress analysis perspective, the FGMO stress result presented in Figure 3 (right side) shows that, at the mid-span (roughly regions 1-2), each layer has constant stress, and stress uniformity is obtained across several layers. This clearly contrasts with the homogenous beam case under pure bending, where, in the elastic range, the normal stresses are known to vary linearly with the distance from the NS. For comparison purposes, the elastic flexure formula $\sigma_{xx} = -My/I$, where M is the bending moment, I is the second moment of area of the beam's cross-section and y is the distance from the NS, is applied here to obtain the maximum absolute value of the normal stress (or flexural stress) in the homogenous beam case presented in Figure 2. This yields $\sigma_{xx} = 2.40$ MPa, considering $M = 100\ \text{kN} \cdot \text{m}$, $I = 1.042 \times 10^{-2}\text{m}^4$ and $y = 0.25$ m. Basically, this means that the FGM beam solution in Figure 3 is 30.8% less stressed than the homogenous beam. The stress analysis here is based on region 1 only, as it is where a well-defined FGM (unidirectional) is caught and responsible for converting the original (linear) stress distribution into a more uniform one.

Noteworthy is also the fact that the FGM solution can increase or decrease compliance

depending on the reference material set for the homogenous beam. For the sake of simplification, the compliance of the beam is computed considering again region 1 only. As regards to the homogenous beam, one obtains $C_1 = 224$ J for $E_1 = 1$ GPa, and $C_2 = 659$ J for $E_2 = 0.34$ GPa. As regards to the FGM beam, one obtains $C_{\text{FGM}} = 471$ J, which falls within the interval $[C_1, C_2]$.

5.2 PROPERTIES POST-PROCESSING

In view of fabrication of the FGM beam solution shown in Figure 3, the layer-wise FGM from region 1 is extended along the entire length of the beam. For that purpose, the discrete Young's Modulus distribution from region 1 is converted into a continuous function that retrieves the Young's Modulus value at any query point within the beam's domain upon definition of its coordinates, specifically the y-coordinate.

To perform the properties' mapping between the FGMO model and a more realistic model for fabrication, the centroid coordinate y of the elements in the FE mesh are firstly listed. Specifically, one focuses on the first half of the elements in the first column of the FE mesh (adjacent to the $y-$axis), which are used as sample points. Basically, the y-coordinate of the centroid of these elements is associated with the respective element's Young's Modulus from the FGMO beam solution, resulting in a stepwise property distribution. Therefore, applying curve fitting to the sample data, a response function for the Young's Modulus [GPa] is generated, i.e., $E(y) = 0.08227y^{-1}$, if $y \in [0.0833;\ 0.25]$, and $E(y) = -0.08227y^{-1}$, if $y \in [-0.25; -0.0833]$. Based on this piecewise function, one can see that the Young's Modulus of the FGMO solution follows a hyperbolic-law. Noteworthy is also the fact that, for the definition of this piecewise function, the origin of the coordinate system is considered to coincide with the intersection of both horizontal (x) and vertical (y) axes of the beam, recall Figure 2. With the definition of $E(y)$, the new Young's Modulus distribution of the FGM beam is straightforwardly obtained. However, note that for elements whose y-coordinate centroid is not within the domain of $E(y)$, the Young's Modulus value is set to $E_1 = 1$ GPa. Finally, Figure 4 shows the Young's Modulus distribution of the FGM beam after the property post-processing just described. The entire FGM beam model is represented in Figure 4.

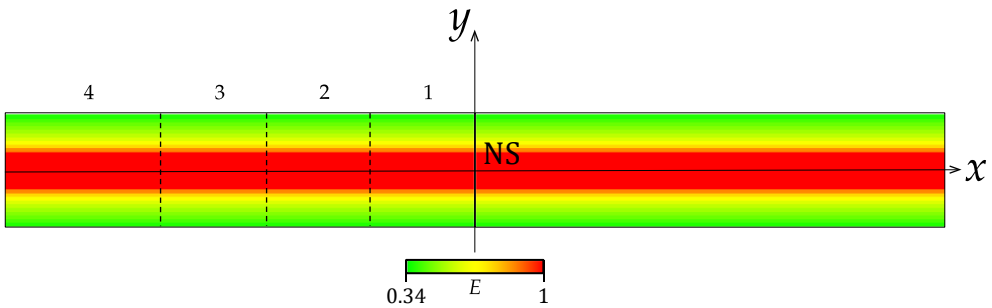

Figure 4 Property post-processing (Young's Modulus) of the FGM beam solution presented in Figure 3.

5.3 STRESS AND DISPLACEMENT ANALYSIS

This section aims to provide a stress and deformed shape analysis of the layer-wise FGM beam solution presented in Figure 4, i.e., after the property post-processing. For this purpose, a FE mesh with the same number of elements, geometric characteristics, boundary conditions, and loading conditions (recall Figure 2) is used. Each FE of the mesh has a Poisson's ratio of 0.3, and the Young's Modulus is computed using the piecewise function $E(y)$, which depends on the elements' centroid coordinate y.

The layer-wise FGM beam is here compared to the single-material counterparts in terms of strength and deformed shape. Figure 5 compares the von Mises stress maps between the layer-wise FGM beam and the homogenous beam using either Mat 1 or Mat 2. For visualization purposes only, elements with higher stress values than those observed in regions 1 and 2 were discarded. The stress map of the FGM beam at mid-span is consistent with the one presented in Figure 3. The highest stress values of both the homogenous and FGM beams are highlighted at the color scale for comparison.

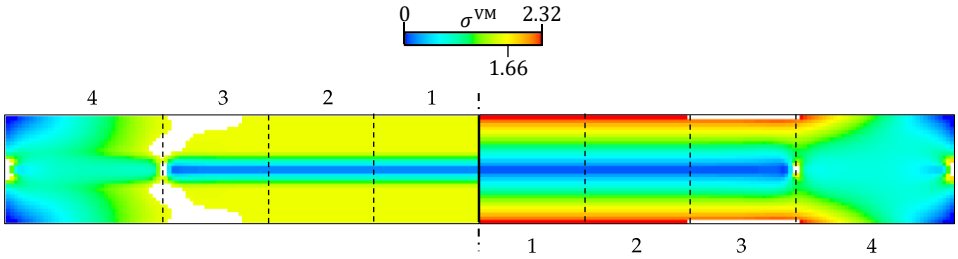

Figure 5 Comparison between the stress maps of the FGM beam (left side) and the homogenous beam (right side).

The deformed shapes of the FGM beam and homogenous beams using Mat 1 and Mat 2 are plotted in Figure 6. Basically, each point plotted corresponds to an element midside node located on the NS of the beam. Consistently, the FGM beam deformed shape lies between those of the homogenous counterparts, as also suggested by the compliance values indicated in Section 5.1. Specifically, the maximum vertical displacement U_y observed in the FGM beam equals -0.044 m, which is 43% lower than that of the homogenous beam using Mat 2 and 51% higher than that of the homogenous beam using Mat 1. As regards to the FGM beam, the transverse displacement u_y analytical expression is given by $u_y(x) = -0{,}00092x^4 + 0{,}00336x^3 + 0{,}00626x^2 + 0{,}00145x - 0{,}04411$ (m). This is here given as reference for comparison purposes with the known analytical homogeneous beam deformed shapes from the literature, also given by polynomial functions.

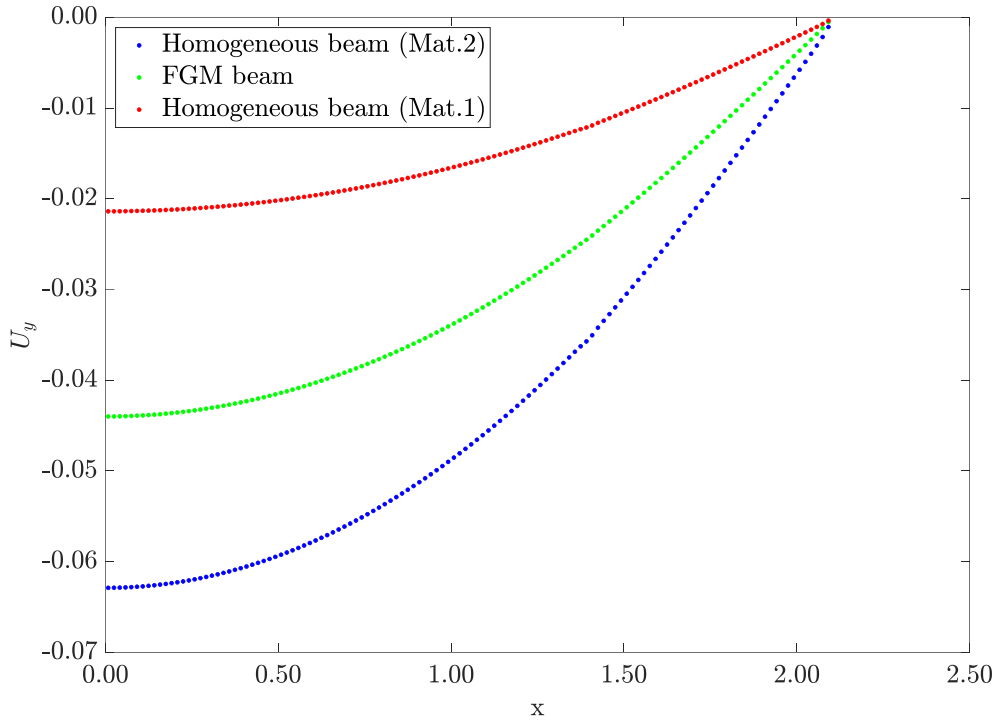

Figure 6 Deformed shapes of the FGM beam and homogenous counterparts.

6 CONCLUSIONS

This research focuses on minimizing stresses within a beam under pure bending utilizing an FGM model. This enlarges the design space, allowing for improved structural performance. The type of FGM addressed in this work involves gradual changes in the volume fraction of the constituent materials such that the heterogeneous resulting beam provides continuous graded macroscopic properties (e.g., Young's Modulus). In the absence of related experimental data, theoretical predictions based on the HS bounds have been consistently used to feed numerical models and optimize structures, as done in this work. In addition, one uses the RAMP interpolation scheme to approximate the average of the HS bounds.

Unlike previous research works, that resort to predefined property gradient models, e.g., exponential or power-law models, the present framework aims to find the optimal property gradient across the beam's domain, thus avoiding a priori any gradient assumption. The design approach proposed here adequately predicts the Young's Modulus gradient to excel in structural performance. In the beam example presented in this work, related pure bending stresses are minimized on account of a layer-wise FGM, where the Young's Modulus variation across the beam's cross-section is given by a hyperbolic-law.

In view of fabrication of the layer-wise FGM beam, the discrete Young's Modulus distribution obtained from the optimization process is converted into a continuous function that retrieves the Young's Modulus value at any query point within the beam's domain upon definition of its coordinates. The properties' mapping between the FGMO model and a more realistic model for fabrication is performed. Stress and deformed shape analyses are performed resorting to a post-processed layer-wise FGM beam.

For future works, several avenues of practical research in materials science and fabrication technologies can be foreseen for materializing FGMs as designed by TO, not forsaking the important metallurgical issues that may arise from combining dissimilar materials.

ACKNOWLEDGMENTS

Authors wish to thank the Portuguese Foundation for Science and Technology, FCT/MCTES-Portugal, for the funding through the projects 2022.06903.PTDC - TOP&AM4FGM (http://doi.org/10.54499/2022.06903.PTDC), UIDB/00667/2020 and UIDP/00667/2020 (UNIDEMI), UIDB/EMS/50022/2020 (IDMEC/LAETA) and the PhD studentship 2021.05360.BD.

REFERENCES

[1] M. Naebe and K. Shirvanimoghaddam. "Functionally graded materials: A review of fabrication and properties.", *Appl. Mater. Today*, vol. 5, pp. 223–245, dez. 2016, doi: 10.1016/j.apmt.2016.10.001.

[2] M. M. J. Opgenoord and K. E. Willcox, "Design for additive manufacturing: cellular structures in early-stage aerospace design.", *Struct. Multidiscip. Optim.*, vol. 60, n.º 2, pp. 411–428, ago. 2019, doi: 10.1007/s00158-019-02305-8.

[3] S. Nikbakht, S. Kamarian, and M. Shakeri, "A review on optimization of composite structures Part II: Functionally graded materials.", *Compos. Struct.*, vol. 214, pp. 83–102, abr. 2019, doi: 10.1016/j.compstruct.2019.01.105.

[4] V. Boggarapu *et al.* "State of the art in functionally graded materials.", *Compos. Struct.*, vol. 262, p. 113596, abr. 2021, doi: 10.1016/j.compstruct.2021.113596.

[5] B. V. Sankar. "An elasticity solution for functionally graded beams.", *Compos. Sci. Technol.*, vol. 61, n.º 5, pp. 689–696, abr. 2001, doi: 10.1016/S0266-3538(01)00007-0.

[6] A. Chakraborty, S. Gopalakrishnan, and J. N. Reddy. "A new beam finite element for the analysis of functionally graded materials.", *Int. J. Mech. Sci.*, vol. 45, n.º 3, pp. 519–539, mar. 2003, doi: 10.1016/S0020-7403(03)00058-4.

[7] R. Kadoli, K. Akhtar, and N. Ganesan. "Static analysis of functionally graded beams using higher order shear deformation theory.", *Appl. Math. Model.*, vol. 32, n.º 12, pp. 2509–2525, dez. 2008, doi: 10.1016/j.apm.2007.09.015.

[8] H. Ziou, H. Guenfoud, and M. Guenfoud. "Numerical modelling of a Timoshenko FGM beam using the finite element method.", *Int. J. Struct. Eng.*, vol. 7, n.º 3, p. 239, 2016, doi: 10.1504/IJSTRUCTE.2016.077719.

[9] F. Althoey and E. Ali. "A Simplified Stress Analysis of Functionally Graded Beams and Influence of Material Function on Deflection.", *Appl. Sci.*, vol. 11, n.º 24, p. 11747, dez. 2021, doi: 10.3390/app112411747.

[10] Y. J. Noh, Y. J. Kang, S. J. Youn, J. R. Cho, and O. K. Lim. "Reliability-based design optimization of volume fraction distribution in functionally graded composites.", *Comput. Mater. Sci.*, vol. 69, pp. 435–442, mar. 2013, doi: 10.1016/j.commatsci.2012.12.003.

[11] A. H. Taheri and B. Hassani. "Simultaneous isogeometrical shape and material design of functionally graded structures for optimal eigenfrequencies.", *Comput. Methods Appl. Mech. Eng.*, vol. 277, pp. 46–80, ago. 2014, doi: 10.1016/j.cma.2014.04.014.

[12] Q. Xia and M. Y. Wang. "Simultaneous optimization of the material properties and the topology of functionally graded structures.", *Comput.-Aided Des.*, vol. 40, n.º 6, pp. 660–675, jun. 2008, doi: 10.1016/j.cad.2008.01.014.

[13] S. Maleki Jebeli and M. Shariat Panahi. "An evolutionary approach for simultaneous optimization of material property distribution and topology of FG structures.", *Eng. Comput.*, vol. 32, n.º 2, pp. 234–257, abr. 2015, doi: 10.1108/EC-07-2013-0188.

[14] S. R. M. Almeida, G. H. Paulino, and E. C. N. Silva. "Layout and material gradation in topology optimization of functionally graded structures: a global–local approach.", *Struct. Multidiscip. Optim.*, vol. 42, n.º 6, pp. 855–868, dez. 2010, doi: 10.1007/s00158-010-0514-x.

[15] J. Cheng, D. Peng, W. Hu, Z. Liu, and J. Tan. "Collaborative robust topology optimization of FGMs considering hybrid bounded uncertainties based on the distance to ideal solution.", *Compos. Struct.*, vol. 341, p. 118205, ago. 2024, doi: 10.1016/j.compstruct.2024.118205.

[16] R. F. Silva, P. G. Coelho, F. M. Conde, B. R. Santos, and J. P. Oliveira. "Minimizing the maximum von Mises stress of elastic continuum structures using topology optimization and additively manufactured functionally graded materials.", *Comput. Struct.*, vol. 301, p. 107469, set. 2024, doi: 10.1016/j.compstruc.2024.107469.

[17] Z. Hashin and S. Shtrikman. "A variational approach to the theory of the elastic behaviour of multiphase materials.", *J. Mech. Phys. Solids*, vol. 11, n.º 2, pp. 127–140, mar. 1963, doi: 10.1016/0022-5096(63)90060-7.

[18] M. Stolpe and K. Svanberg. "An alternative interpolation scheme for minimum compliance topology optimization.", *Struct. Multidiscip. Optim.*, vol. 22, n.º 2, pp. 116–124, set. 2001, doi: 10.1007/s001580100129.

[19] F. M. Conde, P. G. Coelho, and J. M. Guedes. "Multi-material and strength-oriented microstructural topology optimization applied to discrete phase and functionally graded materials.", *Struct. Multidiscip. Optim.*, vol. 65, n.º 4, p. 127, abr. 2022, doi: 10.1007/s00158-022-03209-w.

[20] P. G. Coelho, B. C. Barroca, F. M. Conde, and J. M. Guedes. "Minimization of maximal von Mises stress in porous composite microstructures using shape and topology optimization.", *Struct. Multidiscip. Optim.*, vol. 64, n.º 4, pp. 1781–1799, out. 2021, doi: 10.1007/s00158-021-02942-y.

[21] J. E. Taylor and M. P. Bendsøe. "An interpretation for min-max structural design problems including a method for relaxing constraints.", *Int. J. Solids Struct.*, vol. 20, n.º 4, pp. 301–314, 1984, doi: 10.1016/0020-7683(84)90041-6.

[22] K. Svanberg. "The method of moving asymptotes—a new method for structural optimization.", *Int. J. Numer. Methods Eng.*, vol. 24, n.º 2, pp. 359–373, fev. 1987, doi: 10.1002/nme.1620240207.

[23] E.J. Haug, K.K. Choi, and V. Komkov. “Design sensitivity analysis of structural systems.”, Orlando: Academic Press Inc., 1986.